AIP Publishing

This manuscript was accepted by Appl. Phys. Lett. Click here to see the version of record.

1 # Dislocation Loops as a Mechanism for
2 # Thermoelectric Power Factor Enhancement in
3 # Silicon Nano-Layers

4 *Nick S. Bennett* [a*], *Daragh Byrne* [b], *Aidan Cowley* [c], *Neophytos Neophytou* [d]

5 [a] Nano-Materials Lab., Institute of Mechanical, Process & Energy Engineering, School of
6 Engineering & Physical Sciences, Heriot-Watt University, Edinburgh EH14 4AS, United
7 Kingdom

8 [b] School of Physical Science, Dublin City University, Glasnevin, Dublin 9, Ireland

9 [c] European Astronaut Centre (EAC), European Space Agency (ESA), Linder Höhe, D-51147
10 Cologne, Germany

11 [d] School of Engineering, University of Warwick, Coventry CV4 7AL, United Kingdom

12 [*] Corresponding author, E: n.bennett@hw.ac.uk, T: +44 131 451 4379, F: +44 131 451 3129

13

14 A more than 70% enhancement in the thermoelectric power factor of single-crystal
15 silicon is demonstrated in silicon nano-films, a consequence of the introduction of
16 networks of dislocation loops and extended crystallographic defects. Despite these
17 defects causing reductions in electrical conductivity, carrier concentration and carrier
18 mobility, large corresponding increases in the Seebeck coefficient and reductions in
19 thermal conductivity lead to a significant net enhancement in thermoelectric
20 performance. Crystal damage is deliberately introduced in a sub-surface nano-layer

ACCEPTED MANUSCRIPT

AIP Publishing

This manuscript was accepted by Appl. Phys. Lett. Click here to see the version of record.

21 within a silicon substrate, demonstrating the possibility to tune the thermoelectric
22 properties at the nano-scale within such wafers in a repeatable, large-scale and cost-
23 effective way.

24 The recent global drive to be more efficient in the way we use energy, particularly to reduce the
25 amount of energy that goes to waste, has led to renewed interest in thermoelectrics (TE) for
26 waste heat harvesting. In particular demand are materials that use elements that are less costly,
27 less toxic and more Earth-abundant than the popular TE material bismuth telluride (Bi_2Te_3).
28 Despite requiring the scarce element tellurium, Bi_2Te_3 has significantly better thermoelectric
29 performance than more abundant elemental semiconductors, such as silicon (Si). Three material
30 properties determine this performance – thermal conductivity (κ), Seebeck coefficient (S) and
31 electrical conductivity (σ). These interlinked properties are commonly combined to describe
32 performance in terms of the thermoelectric figure-of-merit (Z), where $Z = S^2\sigma/\kappa$. Bi_2Te_3 has
33 approximately 100-fold better Z than bulk Si [1], but is approximately 30-times more expensive
34 [2]. Therefore developing methods that provide significant gains in the Z of Si offers a potential
35 route to more cost-effective and environmentally friendly thermoelectric devices.

36 Since highly-doped Si (doping ~10^{19} cm^{-3}) possesses S and σ competitive with other TE
37 materials, much recent focus has been on reducing its thermal conductivity, which is too high for
38 most practical applications. It been demonstrated possible via nano-structuring, to vastly reduce
39 κ with little or no degradation of other parameters in structures such as Si nanowires, nanofilms
40 or films containing porosity, periodic voids or vacancies [3-13]. This allows for higher Z and
41 makes nano-structured Si an attractive TE material. Such findings, with variations, have been
42 corroborated by numerous groups worldwide, through both theoretical and experimental studies
43 [3-13].

ACCEPTED MANUSCRIPT

AIP Publishing
This manuscript was accepted by Appl. Phys. Lett. Click here to see the version of record.
ACCEPTED MANUSCRIPT

44 Due to this drastic reduction in κ, which is quickly reaching the amorphous limit, further
45 improvements might come from Si's thermoelectric power factor ($PF = S^2\sigma$), for which to date
46 limited progress has been made. However, a small set of recent studies have demonstrated that a
47 significant improvement in Si's *PF* is sometimes possible for polycrystalline Si [14-16] where
48 built-in potential barriers are created by nano-scale grain boundaries or voids [17], combined
49 with high levels of doping. These potential barriers increase energy filtering and as a
50 consequence, the Si Seebeck coefficient. Our previous work demonstrated that a Seebeck
51 coefficient improvement is also realizable in single-crystal Si nanowires by the introduction of
52 dislocation loops, which also create potential barriers and produce a similar effect [18]. This was
53 so far only demonstrated in n-type material and for relatively lowly-doped Si, where the *PF* is far
54 too low for practical applications.

55 In this current article we report that a significant enhancement in the power factor is also possible
56 for p-type bulk material, and more importantly, with high doping concentrations. Improvements
57 in the *PF* by ~70 % compared to control samples (bulk Si) are realized, giving $PF = 6.6$ mW m^{-1}
58 K^{-2} at 300 K – significantly higher than that of traditional Bi_2Te_3 materials used in current
59 commercial devices.

60 Four different sample types were fashioned from prime <100> single-crystal Si wafers (n-type, 5-
61 10 Ω cm). Ion-implantation of ^{28}Si ions was carried out on a Varian VIISta ion implanter at beam
62 energy 2 MeV. Two wafers received a fluence of 2x10^{15} ions cm^{-2} and two others received
63 6x10^{15} ions cm^{-2}. Wafers received thermal annealing in nitrogen in a furnace at 900°C for a time
64 of either 20 or 60 mins, before being diced into squares. Along with a non-implanted control
65 wafer, samples were then thinned by etching in 25% KOH solution at 60°C, to precisely remove
66 the top 1.5 μm of the wafer. Spin-on dopant (boron) was deposited on each sample before heating

AIP Publishing

This manuscript was accepted by Appl. Phys. Lett. Click here to see the version of record.

67 for 10 mins at 900°C in nitrogen to drive-in the dopant, creating a p-type region with a p/n
68 junction immediately beneath it, isolating the p-type defect-rich nano-layer from the n-type
69 substrate. A dip in HF was applied to remove surface boron-silicate glass. The B doping profile
70 was confirmed as being the same in all samples by differential Hall profiling [19], with a
71 relatively flat doping peak. This confirmed the junction depth as being ~800 nm, to coincide with
72 the bottom of the defective layer and that the thickness of pristine Si remaining at the top of the
73 film was only ~30-45 nm. Fig. 1 provides a schematic illustration of the steps used for sample
74 fabrication.

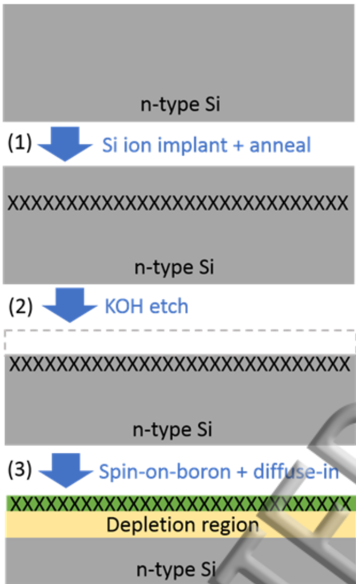

75

76 **Figure 1.** Schematic diagram showing the sample fabrication steps. The Si wafers underwent Si ion-implantation
77 and annealing to create a sub-surface nano-layer rich in defects (represented by Xs). Following removal of the wafer
78 surface by KOH etching, the nano-layer was doped p-type, creating a p/n junction and isolating it from the n-type
79 substrate.

80 Each sample underwent characterization. The presence and nature of defects in the nano-layers
81 were characterized by cross-sectional transmission electron microscopy (XTEM). Micrographs of
82 each of the samples created are presented in Fig. 2. Fig. 2(a) shows the location of the buried

ACCEPTED MANUSCRIPT

AIP Publishing

This manuscript was accepted by Appl. Phys. Lett. Click here to see the version of record.

83 layer relative to the original wafer surface. The remaining micrographs show shows defects
84 created with each of the four implant/annealing conditions. All micrographs show clear evidence
85 of dislocation loops and implantation extended defects, with the higher implant dose creating a
86 higher density of defects. Samples were sent to a commercial vendor for through-plane thermal
87 conductivity measurements. These were extracted by a thermo-reflectance method. Electrical
88 conductivity, Hall-effect and differential Hall measurements were made in air in van der Pauw
89 geometry, using a Biorad HL5900 tool. Temperature-dependent electrical conductivity and
90 Seebeck measurements were made in-plane on a Linseis LSR-3 instrument in He ambient at 10^4
91 Pa.

ACCEPTED MANUSCRIPT

AIP Publishing

This manuscript was accepted by Appl. Phys. Lett. Click here to see the version of record.

92 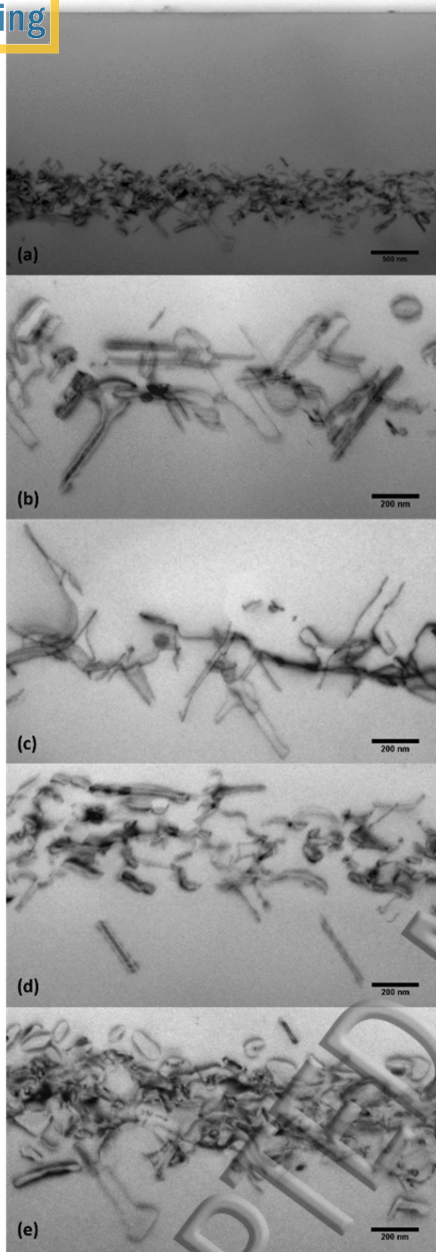

93 **Figure 2.** Micrographs showing sub-surface defect-rich regions created in the Si wafers. (a) Shows the layer
94 location relative to the wafer surface (scale bar is 500 nm). (b) Shows defects created with 2 x 10^{15} cm^{-2} implant,
95 900°C, 20 mins annealing. (c) Shows defects created with 2 x 10^{15} cm^{-2} implant, 900°C, 60 mins annealing. (d)
96 Shows defects created with 6 x 10^{15} cm^{-2} implant, 900°C, 20 mins annealing. (e) Shows defects created with 6 x 10^{15}
97 cm^{-2} implant, 900°C, 60 mins annealing. (Scale bars in (b)-(e) are 200nm).

ACCEPTED MANUSCRIPT

AIP Publishing

This manuscript was accepted by Appl. Phys. Lett. Click here to see the version of record.

98 Fig. 3 shows the variation with implant/annealing conditions for through-plane thermal
99 conductivity at 300 K. κ was 132.6 W m^{-1} K^{-1} for the defect-free control sample and was found
100 to decrease significantly as a result of implantation-induced damage. κ fell to a value of 70.4 W
101 m^{-1} K^{-1} for the lower implantation fluence with 20 min annealing, but recovered slightly to 76.6
102 W m^{-1} K^{-1} following annealing for 60 min. This was an expected result since it is both intuitive
103 and well-established that the introduction of defects within a 'perfect' crystal lattice reduces its
104 thermal transport, and that with longer annealing, more damage will be removed and recovery of
105 thermal transport will occur. For the larger fluence, κ was reduced more, to 43.2 W m^{-1} K^{-1} for
106 20 min annealing and to 48.9 W m^{-1} K^{-1} with 60 min annealing.

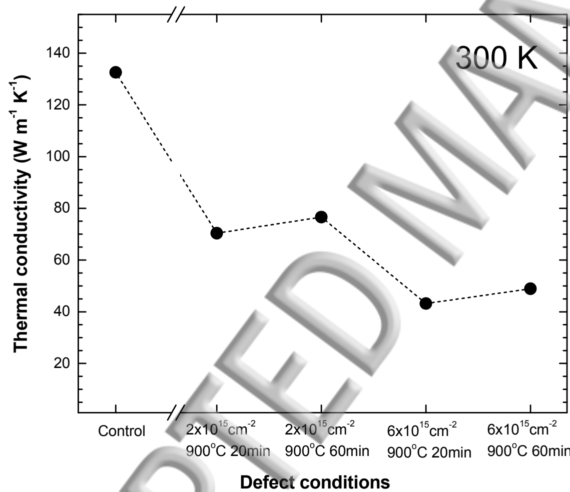

107

108 **Figure 3.** Thermal conductivity (through-plane) as a function of implant/annealing conditions for a control sample
109 relative to samples with 2 MeV Si implant with (i) 2 x 10^{15} cm^{-2} fluence, 900°C, 20 mins annealing, (ii) 2 x 10^{15} cm^{-2}
110 fluence, 900°C, 60 mins annealing, (iii) 6 x 10^{15} cm^{-2} fluence, 900°C, 20 mins annealing, and (iv) 6 x 10^{15} cm^{-2}
111 fluence, 900°C, 60 mins annealing. Measurements were made at 300 K.

112 Fig. 4 shows the change in σ in each sample as a function of the conditions used to create
113 defects. Results are displayed for measurements made at 300, 350 and 400 K, although

ACCEPTED MANUSCRIPT

AIP Publishing

This manuscript was accepted by Appl. Phys. Lett. Click here to see the version of record.

114 differences as a result of temperature were modest in these samples, with only a small
115 conductivity decrease seen in each sample as the measurement temperature is raised. More
116 obvious was the change in conductivity as the implant/annealing conditions were changed.
117 Clearly the control sample had the highest σ of 415 S cm^{-1}. For the lower of the implant fluences,
118 conductivity was reduced relative to the control, and for the higher fluence, conductivity was
119 reduced to less than half. For each fluence, it was the sample that received the shortest anneal
120 that had the lowest conductivity. These trends are intuitive and it is unsurprising that trends in
121 electrical conductivity match those in thermal conductivity (Fig. 3). These trends are similar in
122 magnitude, i.e. as thermal conductivity is reduced for a given condition, so is electrical
123 conductivity by a similar extent, suggesting little net gain in electrical/thermal transport behavior
124 results from the introduction of dislocations, each quantity being reduced by a factor of ~3. It is
125 worth mentioning that XTEM images – particularly Fig. 2(d) and 2(e) – are perhaps deceiving,
126 as one might expect the electrical/thermal conductivity to be lower for the sample in Fig. 2(e)
127 where defects are more apparent. This is opposite to what is measured. In reality, samples having
128 received shorter anneals contain the most defects and lower electrical/thermal conductivity, yet
129 these defects are in the form of smaller Si-interstitial clusters, not visible in the XTEM at its
130 current resolution.

ACCEPTED MANUSCRIPT

AIP Publishing

This manuscript was accepted by Appl. Phys. Lett. Click here to see the version of record.

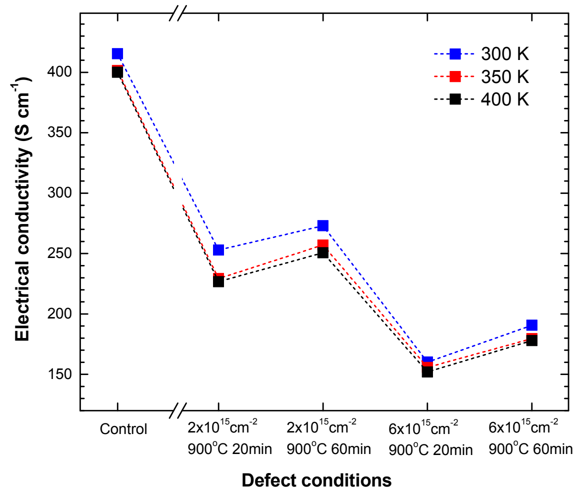

131

132 **Figure 4.** Electrical conductivity (in-plane) as a function of ion-implantation condition and annealing time, for three
133 measurement temperatures (300 K - 400 K).

134 Fig. 5 gives further detail of the room-temperature σ by way of Hall measurement data. Carrier
135 concentration and Hall mobility at 300 K are presented. They show that defect-mediated
136 decreases in σ are a result of a fall in both Hall mobility and carrier concentration, though the
137 former drop is more significant. Crystallographic defects are well known to degrade carrier
138 mobility in Si and this clearly occurs in current samples. B dopant activation is highest in the
139 control sample following drive-in, whereas defects reduce the carrier concentration by up to
140 10%. Since B is well-known to cluster with self-interstitials it is likely that their presence during
141 the drive-in phase means a proportion of the dopants are trapped in inactive clusters rather than
142 finding substitutional sites. B activation improves slightly after longer-duration annealing.

ACCEPTED MANUSCRIPT

AIP Publishing

This manuscript was accepted by Appl. Phys. Lett. Click here to see the version of record.

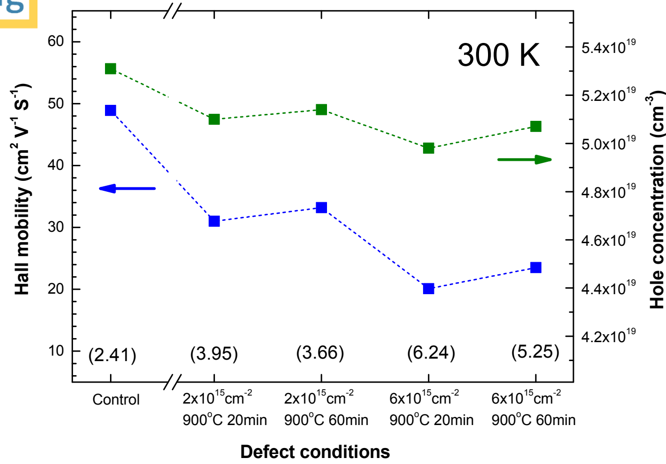

143

144 **Figure 5.** Hall mobility (left axis) and hole concentration (right) as a function of defect conditions. Measurements

145 were made at 300 K. Values in parentheses are corresponding resistivity values in mΩ cm.

146 In-plane Seebeck coefficient measurements were carried out for each of the samples. Results are

147 displayed for measurements made at 300, 350 and 400 K, although as for σ, temperature-

148 dependent differences are modest, with only a small S increase seen in each sample as the

149 measurement temperature is raised. In this case S was lowest in the control sample (Fig. 6(a)),

150 though this was expected since that sample had the highest electrical conductivity and the two

151 parameters are interrelated, with one usually increasing at the expense of the other. Combining

152 the two in the form of the power factor gives an indication of the net thermoelectric performance,

153 with PF = 3.8 mW m^{-1} K^{-2} at 300 K for the control sample (Fig. 6(b)). This PF value is in line

154 with the highest value pristine Si can provide under optimal doping conditions. All other

155 samples, with lower electrical conductivity, have a higher Seebeck coefficient. The two samples

156 receiving the lower implant dose (2x10^{15} cm^{-2}) have modestly higher S that, when combined with

157 σ, result in a significantly lower thermoelectric PF than the control sample. For the higher

158 implant fluence (6x10^{15} cm^{-2}) with 20 min annealing the PF is worse still, since the relatively

ACCEPTED MANUSCRIPT

AIP Publishing

This manuscript was accepted by Appl. Phys. Lett. Click here to see the version of record.

159 small rise in S is more than negated by the much larger drop in σ. An interesting result occurs
160 however, when the higher fluence sample is annealed for longer, resulting in the formation of a
161 dense network of mostly dislocation-loops with diameters roughly between 100 nm and 200 nm
162 (Fig. 2(e)). In this case the increase in S is much greater than for all other samples and bucks the
163 trend, since given its higher electrical conductivity than the previously mentioned sample, one
164 would expect its Seebeck coefficient to decrease. In fact, as the reader can see, not only is the
165 opposite true, but the increase in S is significant. This has a striking effect on the power factor,
166 which is now on average 70% higher than that of the control sample, with PF = 6.6 mW m^{-1} K^{-2}
167 at 300 K.

ACCEPTED MANUSCRIPT

AIP Publishing

This manuscript was accepted by Appl. Phys. Lett. Click here to see the version of record.

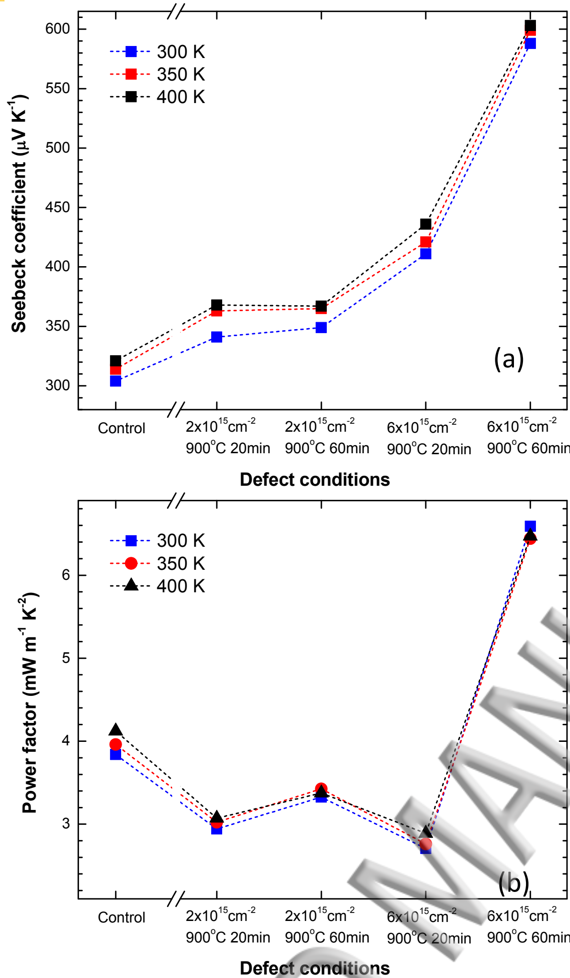

168

169

170 **Figure 6.** (a) Seebeck coefficient (in-plane) and (b) power factor as a function of defect conditions for three

171 measurement temperatures (300 K - 400 K).

172 The simultaneous increase in σ and S is rare, but significant, and results in improved power

173 factors. It is similar to that observed in reference [14] for heavily B-doped nano-crystalline Si,

174 again under high-temperature annealing. While the underlying reasons behind this are still under

175 investigation, it is possible that a number of contributing factors coexist and act synergistically in

176 order to achieve a simultaneous S and σ improvement. For the former, it is probable that

177 potential barriers for holes are created at the dislocation sites, which improve energy filtering and

178 consequently S. Indeed, when present within the crystal lattice, dislocation loops are known to

ACCEPTED MANUSCRIPT

AIP Publishing

This manuscript was accepted by Appl. Phys. Lett. Click here to see the version of record.

179 exert a significant pressure by pushing-apart nearby Si atoms – this pressure increasing the band-
180 gap local to the dislocation site [20]. For the first annealing condition, this local band-gap
181 increase could be responsible for the reduction in conductivity and mobility. As well as allowing
182 loops to form, longer annealing would heal the majority of the Si volume, and thus a slight
183 increase in the electrical conductivity is observed, compensating for any further reduction from
184 the increasing potential barriers. The increased pressure may also improve carrier mobility, a
185 well-known consequence of applying stress in Si [21]. In addition, any local thermal
186 conductivity differences between pristine Si regions and the dislocations might improve S as
187 well. This is because the overall Seebeck coefficient is determined by the weighted average of S
188 in the two regions, with the weighting factor being the temperature drop in each region,
189 determined by their thermal conductivities [14, 22]. Thus, as the crystal lattice is healed,
190 especially in the last annealing step, and local thermal conductivity increases, the local Seebeck
191 coefficient in the dislocation regions (which is expected to be high compared to bulk Si)
192 becomes more important and could warrant the large increase in the overall S observed in Fig.
193 6(a). Our earlier calculations on the effect of filtering by barriers in p-type Si, indicate that
194 filtering alone could provide ~30-40% PF improvements [22, 23], whereas the rest of the
195 measured improvements could originate from the various other factors identified, such as local
196 variations in thermal conductivity and carrier mobility.

197 We have reported a significant enhancement in the power factor of single-crystal Si is
198 possible for highly-doped p-type material, specifically an improvement of ~70 % compared
199 to control samples (bulk Si), giving PF = 6.6 mW m^{-1} K^{-2} at 300 K. This is higher than that
200 of traditional Bi_2Te_3 materials used in commercial thermoelectric devices [24] and is a
201 consequence of the introduction of a dense network of dislocation loops with diameter

ACCEPTED MANUSCRIPT

AIP Publishing

This manuscript was accepted by Appl. Phys. Lett. Click here to see the version of record.

202 between 100 nm and 200 nm. Despite these defects causing reductions in electrical
203 conductivity, carrier concentration and carrier mobility, large corresponding increases in
204 Seebeck coefficient and reductions in thermal conductivity lead to a significant net
205 enhancement in thermoelectric performance. This finding provides a route to significant
206 gains in the thermoelectric power factor of Si, a material that potentially offers a path to
207 more cost-effective and environmentally-friendly thermoelectric devices.

208 **Acknowledgements**

209 NSB, DB and AC thank Science Foundation Ireland for partial support of this work through
210 grant 12/TIDA/E2378 and the Royal Society for supporting research exchange through grant
211 IE131212. NN acknowledges funding from the European Research Council (ERC) under the
212 European Union's Horizon 2020 research and innovation programme (grant agreement No
213 678763). Dr Jan-Willem Bos of Heriot-Watt University is gratefully acknowledged for access to
214 Seebeck measurement facilities.

215 **References**

216 [1] L. Weber and E. Gmelin, Transport properties of silicon. Appl. Phys. A 53 (1991) 136–140.

217 [2] S. Leblanc, S. K. Yee, M. L. Scullin, C. Dames, and K. E. Goodson, Material and
218 manufacturing cost considerations for thermoelectrics, Renewable and Sustainable Energy
219 Reviews 32 (2014) 313.

220 [3] A. I. Hochbaum, R. Chen, R. D. Delgado, W. Liang, E. C. Garnett, M. Najarian, A.
221 Majumdar, and P. D. Yang, Enhanced thermoelectric performance of rough silicon nanowires,
222 Nature 451 (2008) 163–167.

ACCEPTED MANUSCRIPT

AIP Publishing

This manuscript was accepted by Appl. Phys. Lett. Click here to see the version of record.

223 [4] A. I. Boukai, Y. Bunimovich, K. J. Tahir, J. Yu, W. A. Goddard, and J. R. Heath, Silicon
224 nanowires as efficient thermoelectric materials, Nature 451 (2008) 168–171.

225 [5] G. Pennelli, and M. Macucci, Optimization of the thermoelectric properties of nanostructured
226 silicon, J. Appl. Phys. 114 (2013) 214507.

227 [6] E. B. Ramayya, L. N. Maurer, A. H. Davoody, and I. Knezevic, Thermoelectric properties of
228 ultrathin silicon nanowires, Phys. Rev. B 86 (2012) 115328.

229 [7] I. Bejenari and P. Kratzer, Atomistic calculation of the thermoelectric properties of Si
230 nanowires, Phys. Rev. B 90 (2014) 045429.

231 [8] W. Liu, K. Etessam-Yazdani, R. Hussin, and M. Asheghi, Modeling and Data for Thermal
232 Conductivity of Ultrathin Single-Crystal SOI Layers at High Temperature. IEEE Transactions on
233 electron devices 53 (8) (2006) 1868.

234 [9] J. Tang, H. Wang, D. H. Lee, M. Fardy, Z. Huo, T. P. Russell, and P. Yang, Holey silicon as
235 an efficient thermoelectric material, Nano Lett. 10 (2010) 4279-4283.

236 [10] J.-K. Yu, S. Mitrovic, D. Tham, J. Varghese, and J. R. Heath, Reduction of thermal
237 conductivity in phononic nanomesh structures, Nature Nanotechnology 5 (2010) 718–721.

238 [11] P. E. Hopkins, C. M. Reinke, M. F. Su, R. H. Olsson III, E. A. Shaner, Z. C. Leseman, J. R.
239 Serrano, L. M. Phinney, and I. El-Kady, Reduction in the Thermal Conductivity of Single
240 Crystalline Silicon by Phononic Crystal Patterning, Nano Lett. 11 (2011) 107-112.

241 [12] B. Xu and K. Fobelets, Spin-on-doping for output power improvement of silicon nanowire
242 array based thermoelectric power generators, J. Appl. Phys. 115 (2014) 214306.

ACCEPTED MANUSCRIPT

AIP Publishing

This manuscript was accepted by Appl. Phys. Lett. Click here to see the version of record.

243 [13] N. S. Bennett, N. W. Wight, S. R. Popuri, and J.-W. G. Bos, Efficient thermoelectric
244 performance in silicon nano-films by vacancy-engineering, Nano Energy 16 (2015) 350-356.

245 [14] N. Neophytou, X. Zianni, H. Kosina, S. Frabboni, B. Lorenzi, and D. Narducci,
246 Simultaneous increase in electrical conductivity and Seebeck coefficient in highly Boron-doped
247 nanocrystalline Si, Nanotechnology 24 (2013) 205402.

248 [15] N. Neophytou, X. Zianni, H. Kosina, S. Frabboni, B. Lorenzi, and D. Narducci, Power
249 factor enhancement by inhomogeneous distribution of dopants in two-phase nanocrystalline
250 systems, Journal of Electronic Materials 43 (6) (2014) 1896-1904.

251 [16] D. Narducci, B. Lorenzi, X. Zianni, N. Neophytou, S. Frabboni, G. C. Gazzadi, A.
252 Roncaglia, and F. Suriano, Enhancement of the power factor in two-phase silicon-boron
253 nanocrystalline alloys, Physica status solidi a 211 (6) (2014) 1255-1258.

254 [17] B. Lorenzi , D. Narducci, R. Tonini, S. Frabboni, G.C. Gazzadi, G. Ottaviani, N.
255 Neophytou, X. Zianni, Paradoxical enhancement of the power factor in polycrystalline silicon
256 due to the formation of nanovoids, Journal of Electronic Materials 43 (10) (2014) 3812-3816.

257 [18] N. S. Bennett, D. Byrne and A. Cowley, Enhanced Seebeck coefficient in silicon nanowires
258 containing dislocations, Appl. Phys. Lett. 107 (2015) 013903.

259 [19] N. S. Bennett and N. E. B. Cowern, Doping characterization for germanium-based
260 microelectronics and photovoltaics using the differential Hall technique, Appl. Phys. Lett. 100
261 (2012) 172106.

262 [20] K. P. Homewood and M. A. Lourenço, Light from Si via dislocation loops, Materials Today
263 8 (1) (2005) 34-39.

ACCEPTED MANUSCRIPT

AIP Publishing

This manuscript was accepted by Appl. Phys. Lett. Click here to see the version of record.

264 [21] M. L. Lee, E. A. Fitzgerald, M. T. Bulsara, M. T. Currie and A. Lochtefeld, Strained Si,
265 SiGe, and Ge channels for high-mobility metal-oxide-semiconductor field-effect transistors, J.
266 Appl. Phys. 97 (2005) 011101.

267 [22] R. Kim and M. S. Lundstrom, Computational study of energy filtering effects in one-
268 dimensional composite nano-structures, J. Appl. Phys. 111 (2012) 024508.

269 [23] N. Neophytou and H. Kosina, Optimizing Thermoelectric Energy Filtering by Means of a
270 Potential Barrier, J. Appl. Phys., 114 (2013) 044315.

271 [24] “Thermoelectric Energy Harvesting 2016-2026: Devices, Applications, Opportunities”,
272 IDTechEx Report by H. Zervos, updated June 2016, www.idtechex.com

ACCEPTED MANUSCRIPT

n-type Si

XXXXXXXXXXXXXXXXXXXXXXXXXXXXX

n-type Si

XXXXXXXXXXXXXXXXXXXXXXXXXXXXX

n-type Si

XXXXXXXXXXXXXXXXXXXXXXXXXXXXX

Depletion region

n-type Si

ACCEPTED MANUSCRIPT

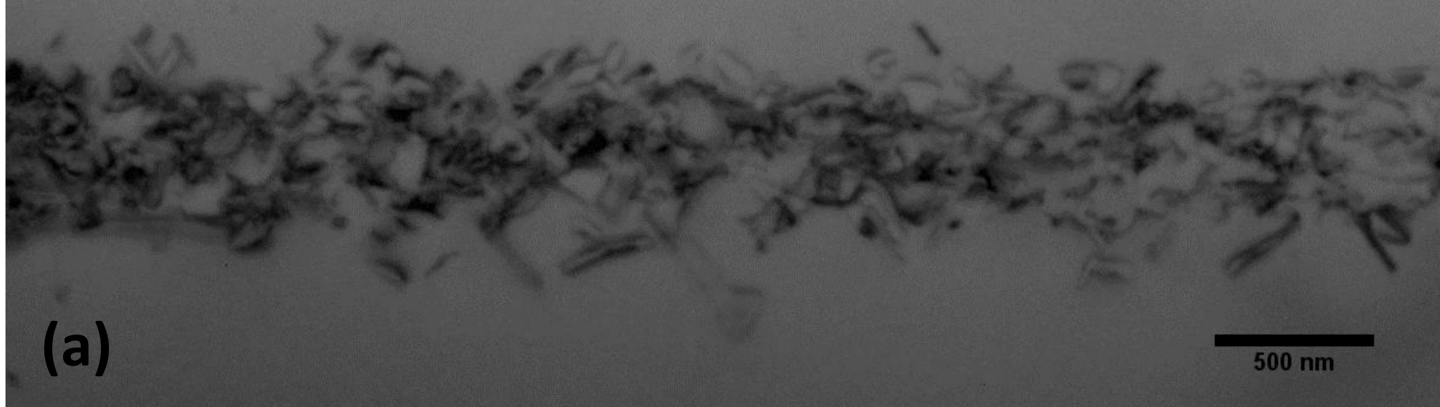

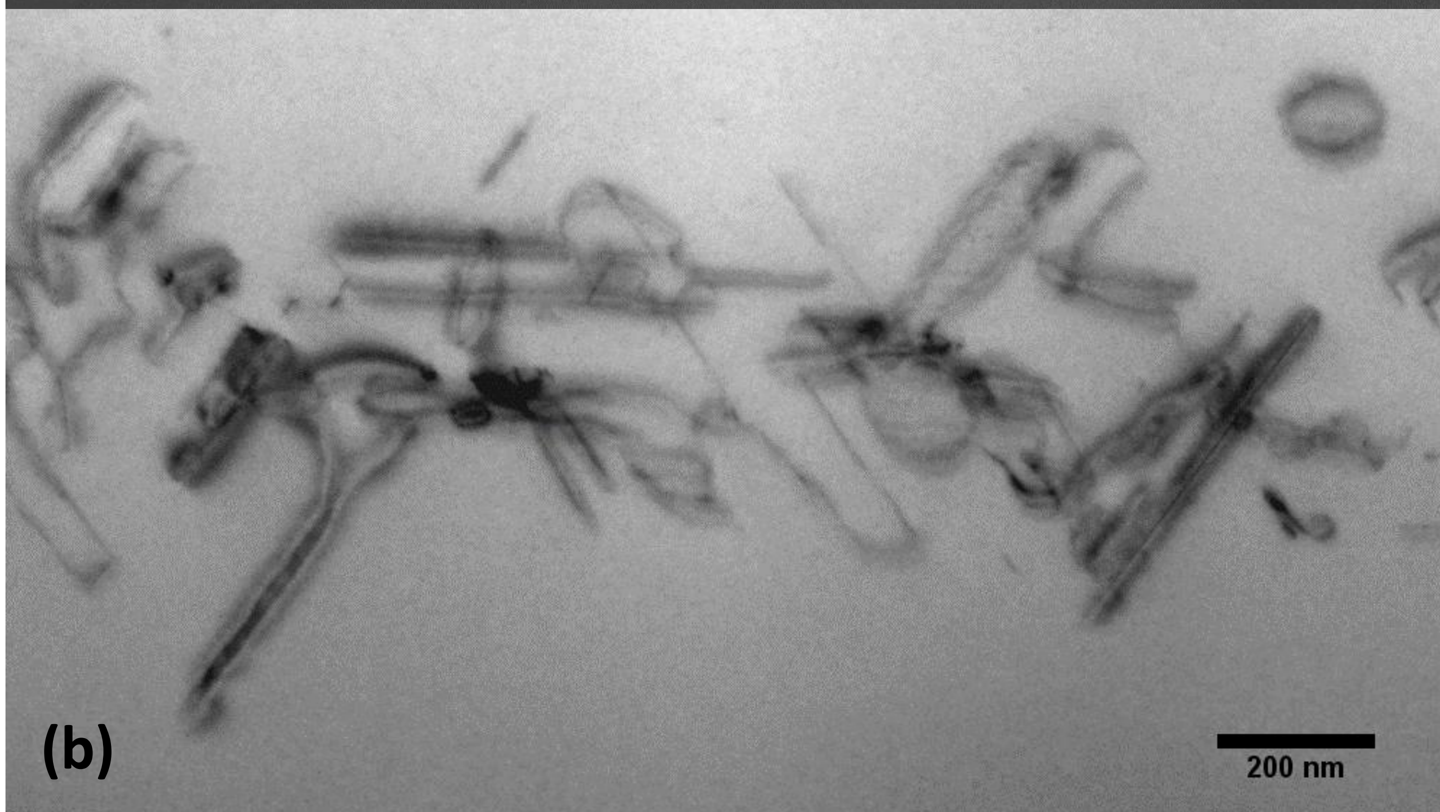

This manuscript was accepted by Appl. Phys. Lett. Click here to see the version of record.

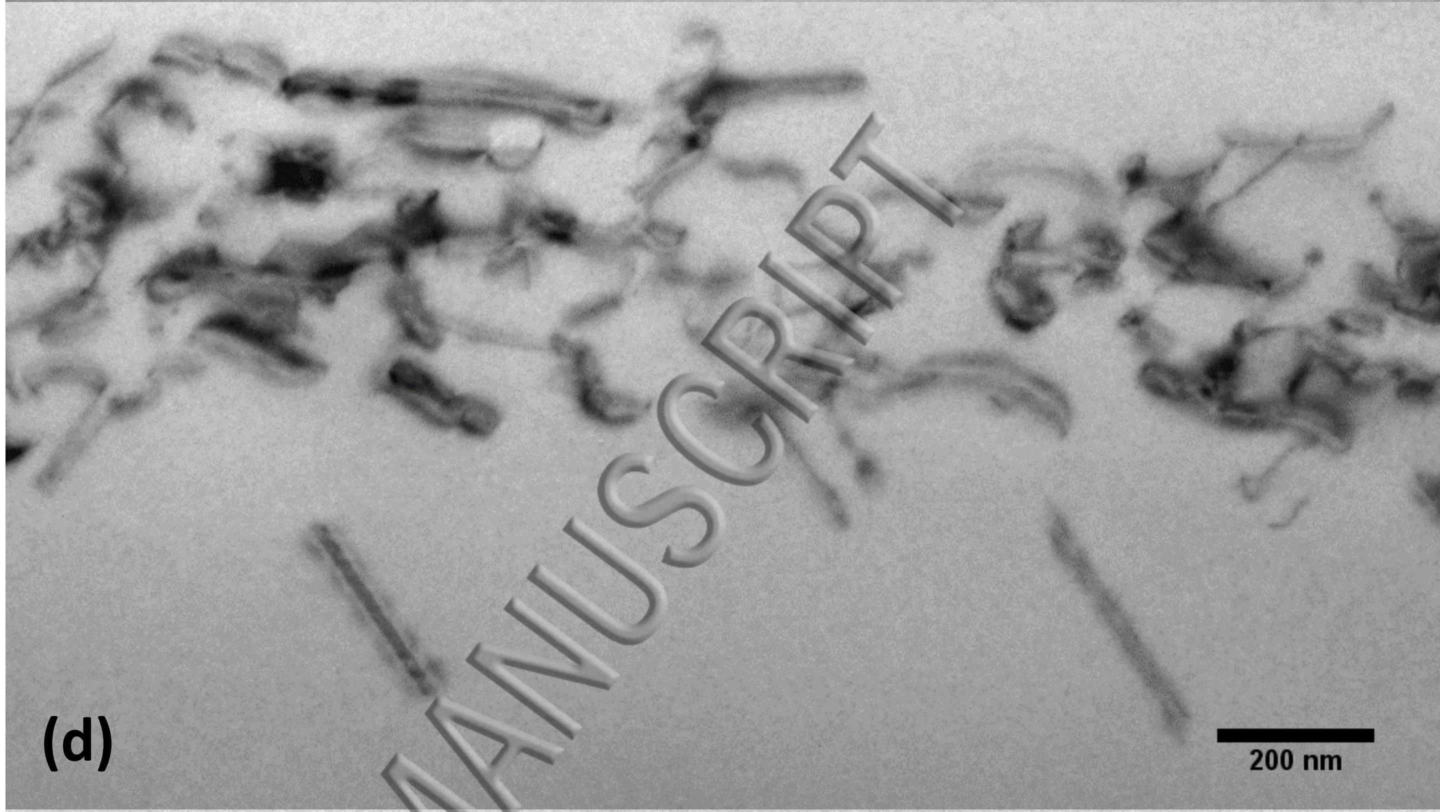

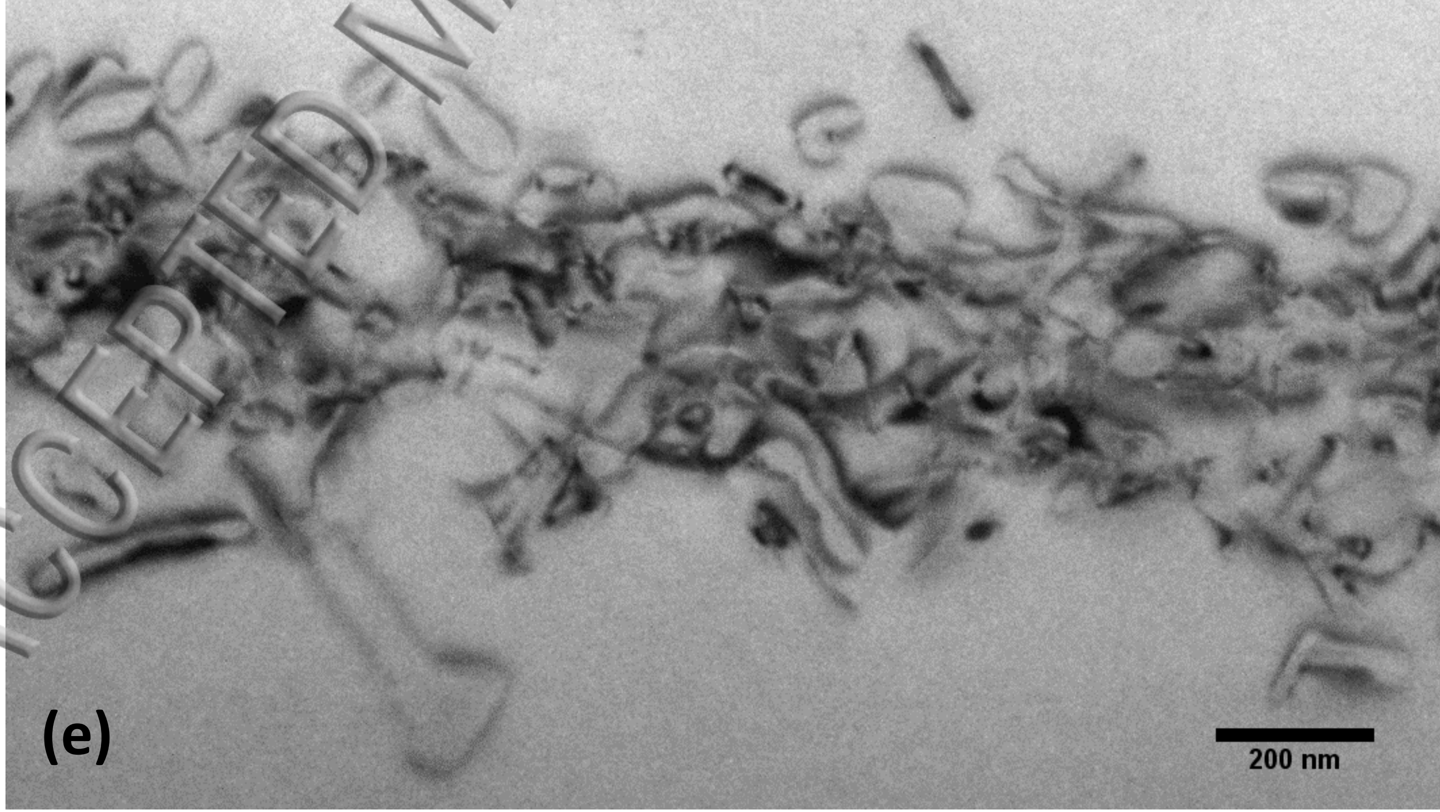

ACCEPTED MANUSCRIPT

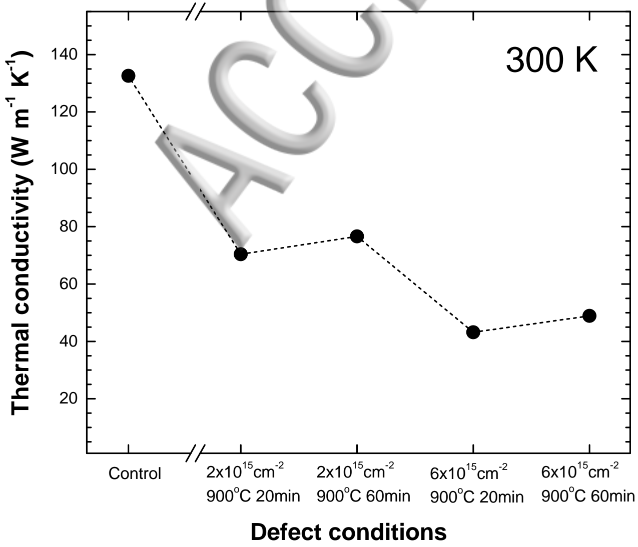
300 K
Thermal conductivity (W m-1 K-1)
140
120
100
80
60
40
20
Control
2x10^15 cm^-2 900°C 20min
2x10^15 cm^-2 900°C 60min
6x10^15 cm^-2 900°C 20min
6x10^15 cm^-2 900°C 60min
Defect conditions

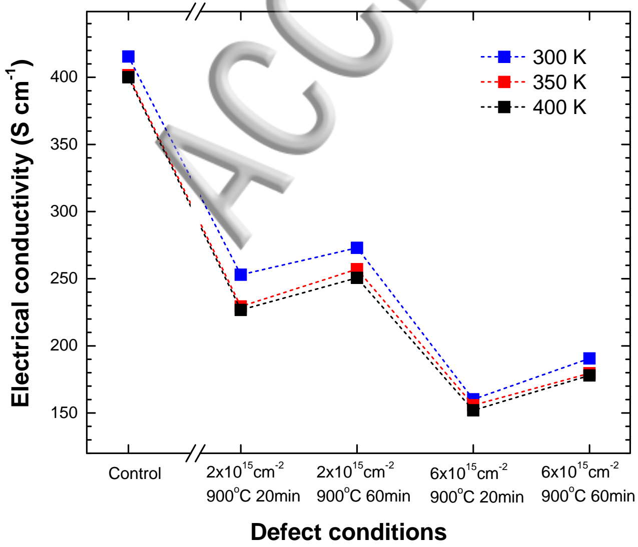

300 K
350 K
400 K
Electrical conductivity (S cm^{-1})
400
350
300
250
200
150
Control
2x10^{15}cm^{-2} 900°C 20min
2x10^{15}cm^{-2} 900°C 60min
6x10^{15}cm^{-2} 900°C 20min
6x10^{15}cm^{-2} 900°C 60min
Defect conditions

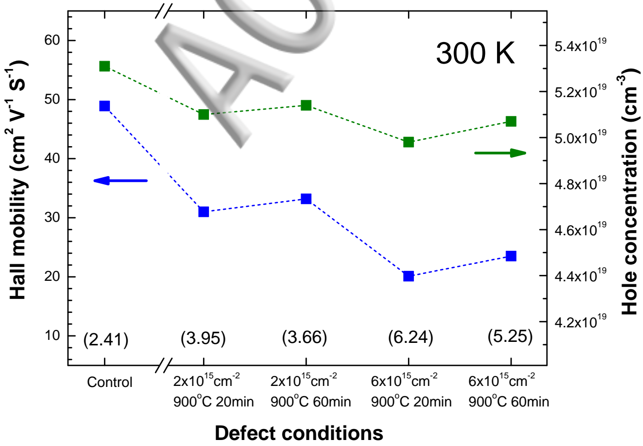
300 K
Hall mobility (cm² V⁻¹ S⁻¹)
Hole concentration (cm⁻³)
60
50
40
30
20
10
5.4x10¹⁹
5.2x10¹⁹
5.0x10¹⁹
4.8x10¹⁹
4.6x10¹⁹
4.4x10¹⁹
4.2x10¹⁹
(2.41)
(3.95)
(3.66)
(6.24)
(5.25)
Control
2x10¹⁵cm⁻² 900°C 20min
2x10¹⁵cm⁻² 900°C 60min
6x10¹⁵cm⁻² 900°C 20min
6x10¹⁵cm⁻² 900°C 60min
Defect conditions

Seebeck coefficient ($\mu V K^{-1}$)

600
550
500
450
400
350
300

300 K
350 K
400 K

(a)

Control
$2x10^{15} cm^{-2}$ 900°C 20min
$2x10^{15} cm^{-2}$ 900°C 60min
$6x10^{15} cm^{-2}$ 900°C 20min
$6x10^{15} cm^{-2}$ 900°C 60min

Power factor ($mW m^{-1} K^{-2}$)

6
5
4
3

300 K
350 K
400 K

(b)

Control
$2x10^{15} cm^{-2}$ 900°C 20min
$2x10^{15} cm^{-2}$ 900°C 60min
$6x10^{15} cm^{-2}$ 900°C 20min
$6x10^{15} cm^{-2}$ 900°C 60min

Defect conditions

ACCEPTED